URA

WASHINGTON UNIVERSITY
DEPARTMENT OF PHYSICS
LABORATORY FOR ULTRASONICS
St. Louis, Missouri 63130

"Non-Destructive Evaluation of Composite Materials Using Ultrasound"

Semiannual Progress Report: September 15, 1983 - March 15, 1984

NASA Grant Number: NSG-1601

Principal Investigator:
Dr. James G. Miller
Professor of Physics

The NASA Technical Officer for this grant is:

Dr. Joseph S. Heyman
NASA Langley Research Center
Hampton, Virginia

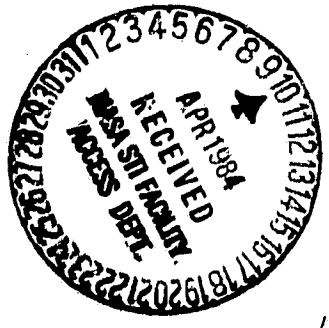

I. INTRODUCTION

This report summarizes our continuing investigation of the non-destructive evaluation of advanced composite-laminates. Our approach makes use of indices derived from the measurement of fundamental acoustic parameters in order to quantitatively estimate the local material properties of the laminate. The following sections describe ongoing studies of phase insensitive attenuation measurements, and discuss several phenomena which may influence the previously reported technique of polar backscatter. A simple and effective programmable gate circuit designed for use in estimating attenuation from backscatter is described in Section IV.

II. Transmission Studies

Previous reports from this laboratory have described experimental systems for the measurement of the attenuation in advanced composite materials by transmission of ultrasound. The procedure for phase-insensitive measurement of the attenuation in transmission has now been implemented on a LSI 11/23 computer system described in previous reports. The entire measurement process can now be selected and monitored from a computer terminal in the laboratory. As the data from each site is recorded, the slope and intercept of the attenuation versus frequency curve is calculated and displayed for the operator's information. The use of the 11/23 computer system greatly speeds the acquisition and analysis of transmission data.

Current studies are under way to demonstrate that the transmission techniques which we described previously are reproducible, investigator-independent, and quantitative. In addition, we are engaged in a further study of the large body of data acquired from transmission measurements performed on glass-epoxy composites in order to clarify the significance of the intercept of the attenuation versus frequency curve, especially in regard to (more conventional) single frequency imaging as compared to slope imaging.

III. EFFECTS OF MODE CONVERSION

The potentially significant tool for non-destructive evaluation provided by the polar backscatter technique requires a re-examination of the phenomena of mode conversion of sound waves at liquid/solid interfaces. As we reported previously, insonifying a composite laminate at nonperpendicular incidence allows the selective interrogation of internal structures, relatively independent of surface reflection effects. The orientation of a polar backscatter coordinate system is shown in Figure 1, in which the polar angle θ, and the azimuthal angle ϕ are defined.

Any configuration in which an initially longitudinal wave in a liquid is incident on a solid at a nonperpendicular angle leads to a redistribution of power between the reflected longitudinal mode and the two transmitted modes, longitudinal and transverse. An analysis of this redistribution is required for proper interpretation of the energy backscattered from internal structures.

The reflection and transmission coefficients for liquid-solid mode conversion of plane waves in homogeneous media are available in the literature.[1,2] We have verified that the results obtained by these authors are equivalent after appropriate algebraic and trigonometric manipulation. We denote the pertinent angles by θ_i for the reflected mode, θ_2 for the transmitted longitudinal mode, and γ for the transmitted transverse mode. These angles are related by Snell's law, as shown in Figure 2. The power in each mode can be represented as follows.

$$R = \left[\frac{Z_1 \cos^2 2\gamma + Z_t \sin^2 2\gamma - Z_1}{Z_1 \cos^2 2\gamma + Z_t \sin^2 2\gamma + Z_1}\right]^2$$

$$T_L = \frac{4\, Z_1\, Z_1 \cos^2 2\gamma}{\left[Z_1 \cos^2 2\gamma + Z_t \sin^2 2\gamma + Z_1\right]^2}$$

$$T_t = \frac{4\, Z_1\, Z_t \sin^2 2\gamma}{\left[Z_1 \cos^2 2\gamma + Z_t \sin^2 2\gamma + Z_1\right]^2}$$

where R is the reflection coefficient for longitudinal waves, T_L and T_t

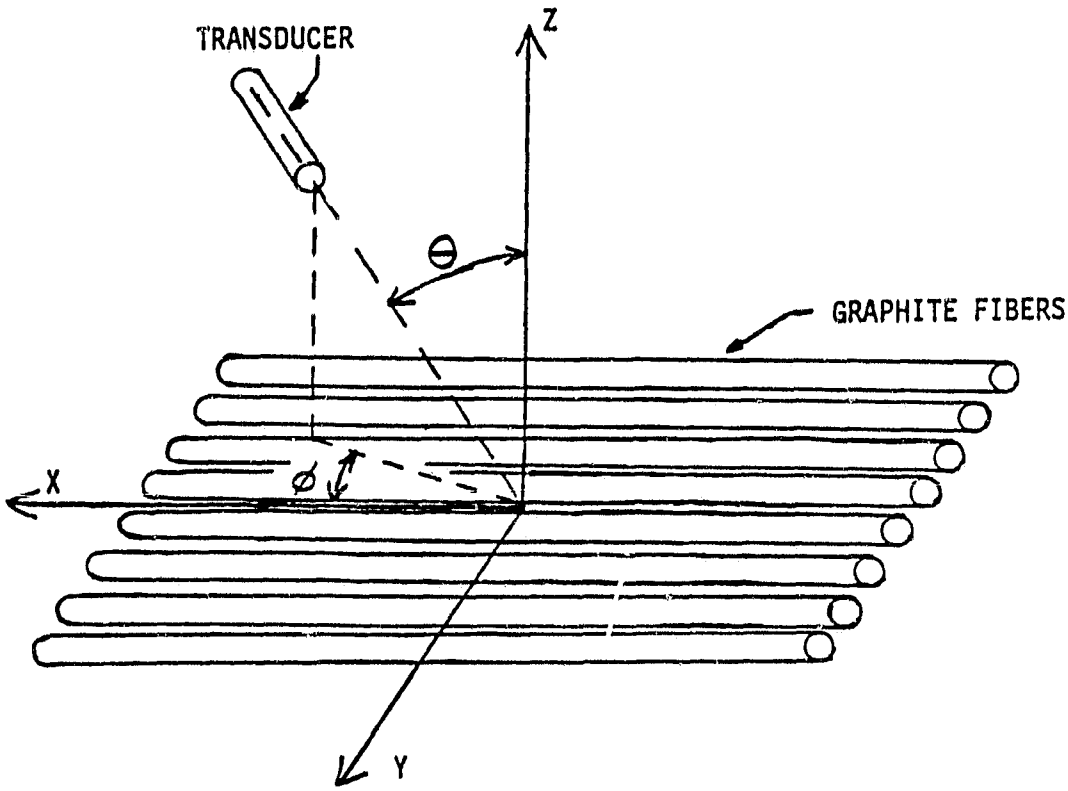

Figure 1. Geometry for measuring polar backscatter. The polar angle (θ) and the azimuthal angle (ø) are measured as shown. In this figure only one fiber orientation is shown; the azimuthal angle is always measured relative to the same fiber orientation.

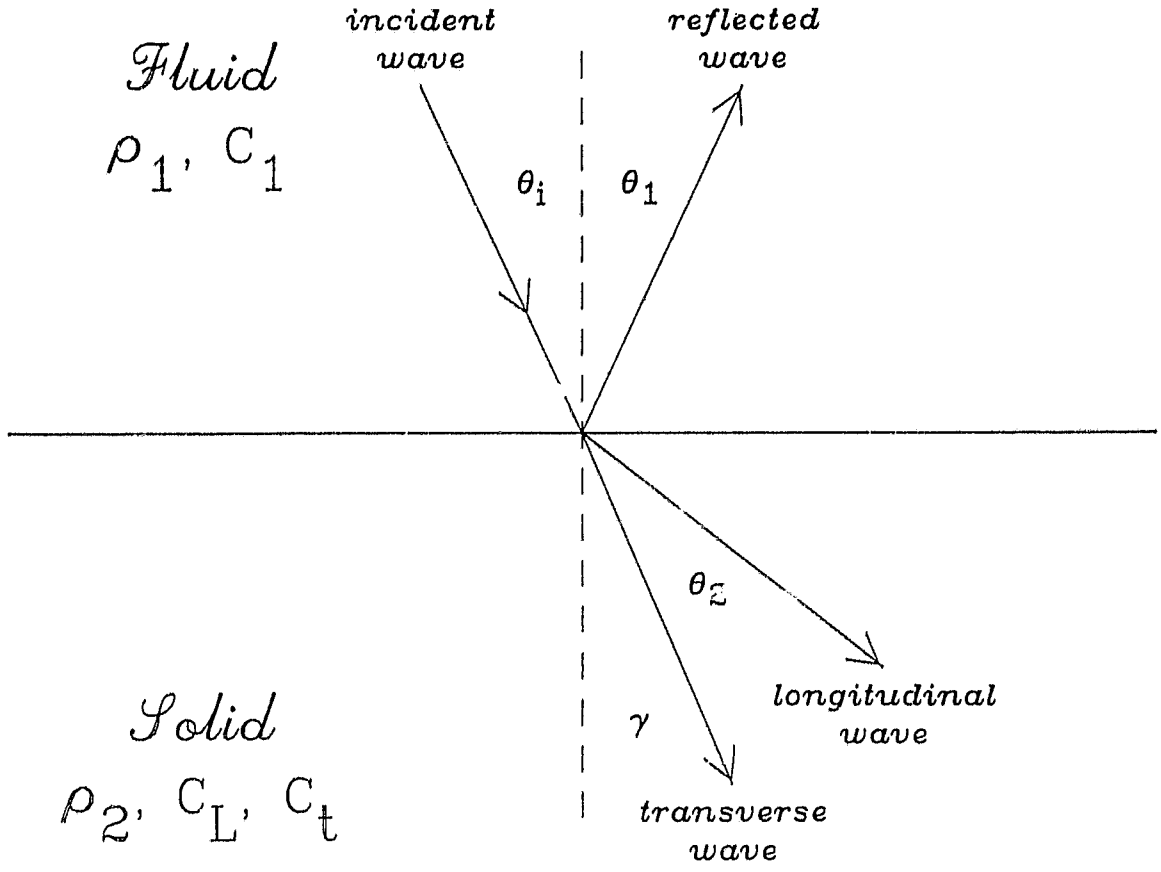

Figure 2 – Angles of mode converted waves according to Snell's Law. Epoxy properties used with $\theta_i = 25°$

are the transmission coefficients for longitudinal and transverse waves, respectively, and Z represents an acoustic impedance defined by

$$Z_i = \frac{\rho_i c_i}{\cos\theta_i}$$

When θ exceeds $\theta_{critical}$, the longitudinal mode becomes imaginary, and is sometimes described as an "inhomogeneous wave". Letting $\cos\theta_2 = i|\cos\theta_2|$ and complex conjugating appropriately, the power in the transverse and reflected mode are easily reformulated from the above expressions.

Using published values for velocities in a typical epoxy,[3] we calculated the distribution of power for plane wave mode conversion (Figure 3). The exchange of energy from the transmitted longitudinal mode into the transmitted transverse mode is apparent as θ increases from zero degrees. Near the longitudinal critical angle of 32.4 degrees, the reflected mode dominates. For $\theta > 33$ degrees, the shear mode dominates.

Clearly this formulation is limited in several regards. First, no account has been taken of the energy converted into Rayleigh surface waves, a mode which is certainly important when $\theta > \theta_{critical}$. Secondly, the formulation does not deal explicitly with frequency dependent phenomena. (Ngoc and Mayer[2] have included frequency dependent attenuation effects for monochromatic reflection and transmission.) Finally, physical transducers do not produce "pure" plane waves, even in the focal zone. A useful representation is a superposition of an angular distribution of plane waves.[2,4] This superposition accounts for the finite beam width, and nearly plane wave behavior in the focal zone. Some of the implications of these considerations will be discussed later in this report.

In order to relate the considerations above to practical ultrasonic measurements, we used a 1.2 mm diameter piezoelectric receiver to determine the beam profile of a 5 MHz focused transducer before and after a plastic specimen was inserted in the beam. The receiving transducer was scanned in a line perpendicular to the transmitter under control of the

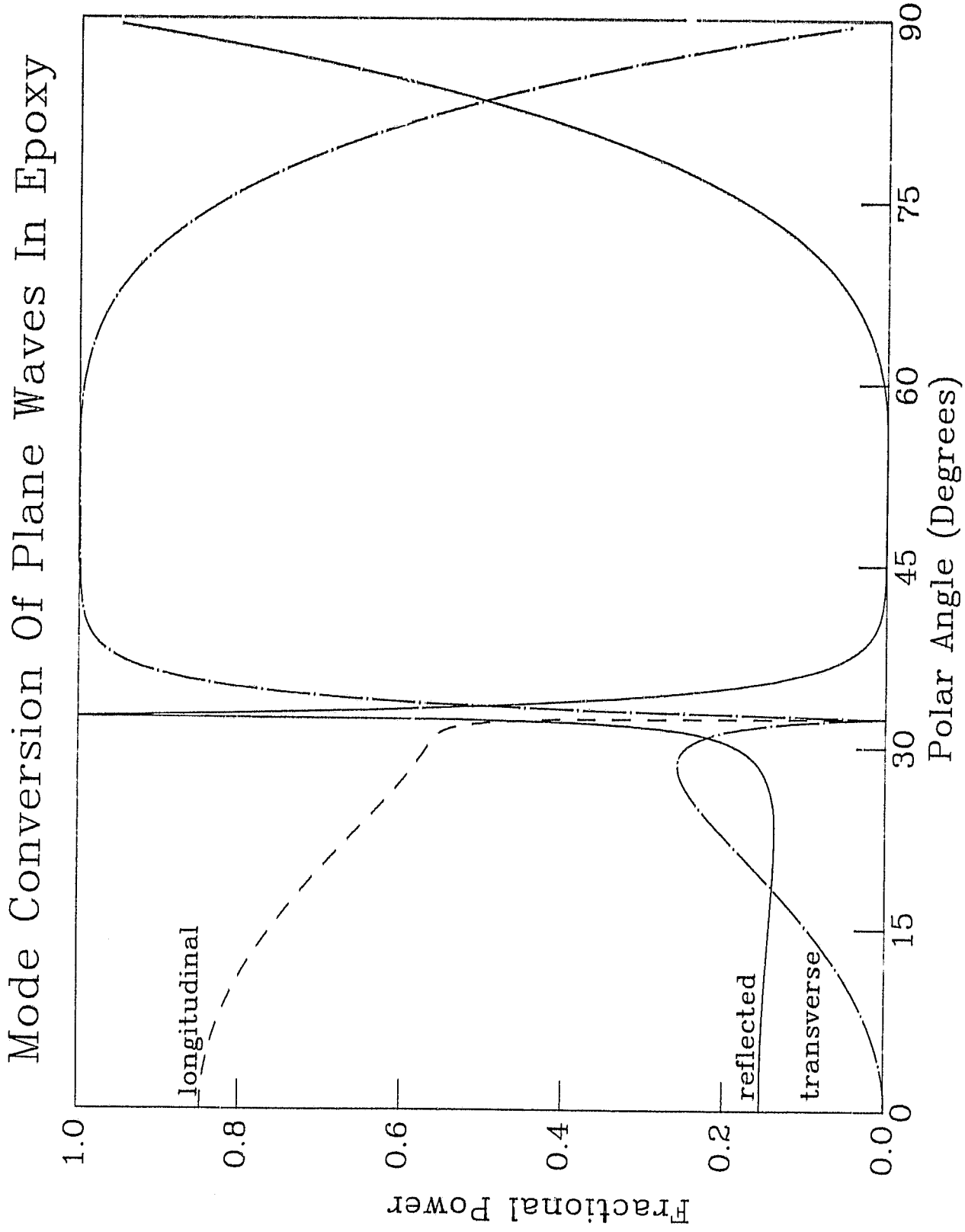

Figure 3 – Distribution of power for mode conversion at water/epoxy interface.

PDP 11/23 computer system described in previous progress reports. A selected portion of the received signal was gated into a spectrum analyzer. The 6 MHz component was read by the computer and stored on disc for later processing. A 5 mm thick slab of Lucite was then introduced between the transducers, which were mounted to allow rotation of the slab to achieve various incident angles. The thickness of the slab was chosen based on handbook[5] values of the velocities in Lucite. Simple calculations showed that this thickness would result in a sufficient time separation of any transverse waves from the faster longitudinal waves.

Figure 4 compares the beam profile measured with a water-only configuration to the beam profile obtained after transmission through the plastic at normal incidence. The horizontal scale on this and the subsequent four figures represent the lateral dimensions of the scan line. Although the absolute origin of the horizontal axis varies in some figures, the scale size is unchanged. The backscatter was calibrated in dB relative to the central peak of the beam. The water-only profile was calibrated relative to its peak. All other profiles were calibrated in terms of the central peak of the normal incidence($\theta = 0$ degrees) transmitted profile, which was 58 dB below that of the water-only profile. For convenience, the 58 dB difference is omitted in Figure 4. We note that after the beam was transmitted through the plastic plate at normal incidence, the relative shape of the beam was essentially unchanged from that exhibited by transmission through a water-only path, except that the sidelobes are about 5 dB higher(with respect to the main lobe) after insertion of the Lucite.

After a rotation of the sample to an incident angle of 50 degrees, the critical angle of 34 degrees is definitely exceeded; no signal is observable at the arrival time of any longitudinal modes. Thus, the beam profile of the transverse mode should contain almost all the energy transmitted into the sample. In Figure 5 the pure L-wave profile shown in Figure 4 is compared with the pure T-wave observed at 50 degrees. To facilitate comparison, the profiles have been aligned horizontally, since the shear wave experiences refraction. The profiles are similar,

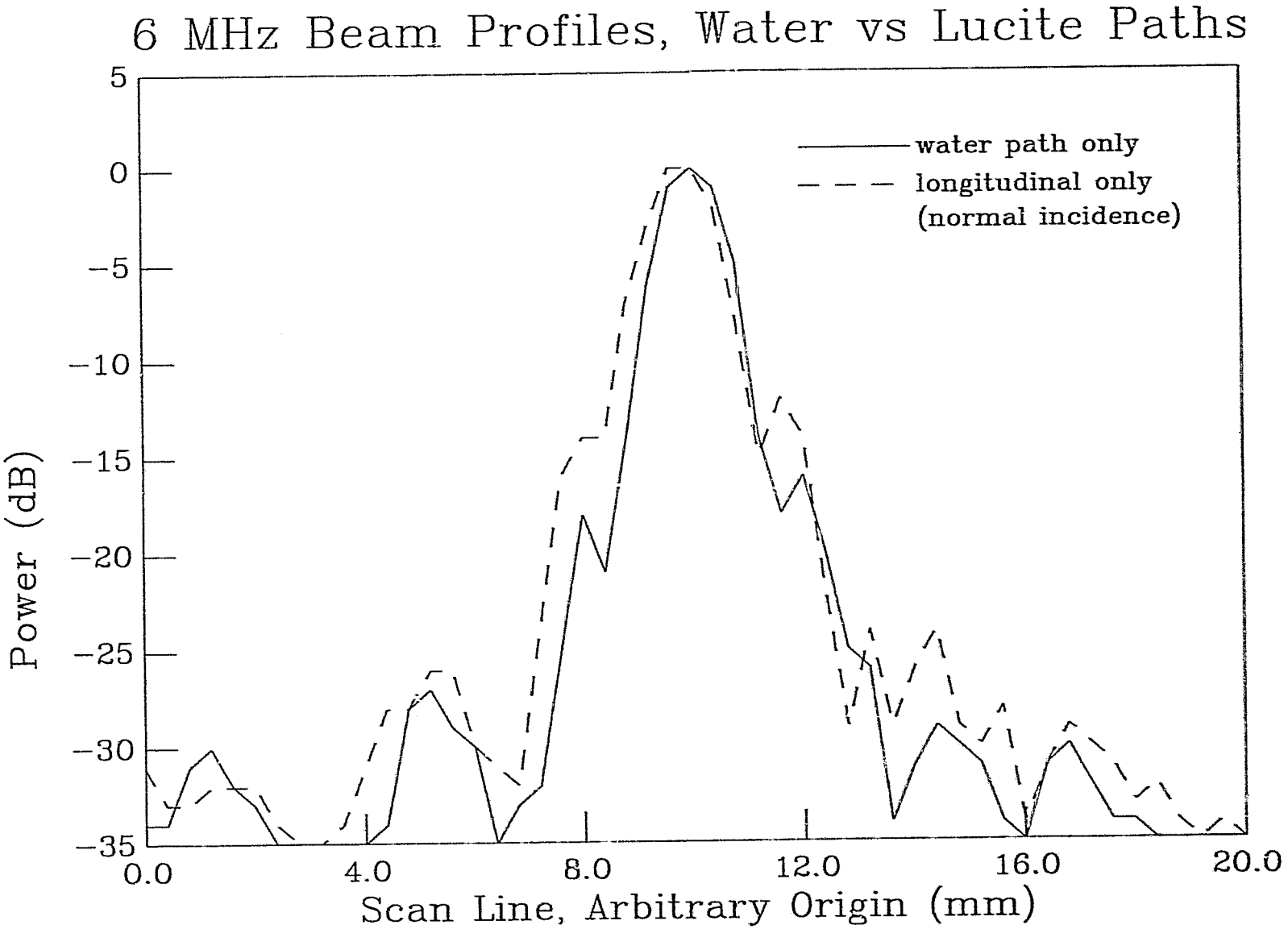

Figure 4 – Normalized comparison of the beam profile after transmission through Lucite (0° incidence) to a water only path

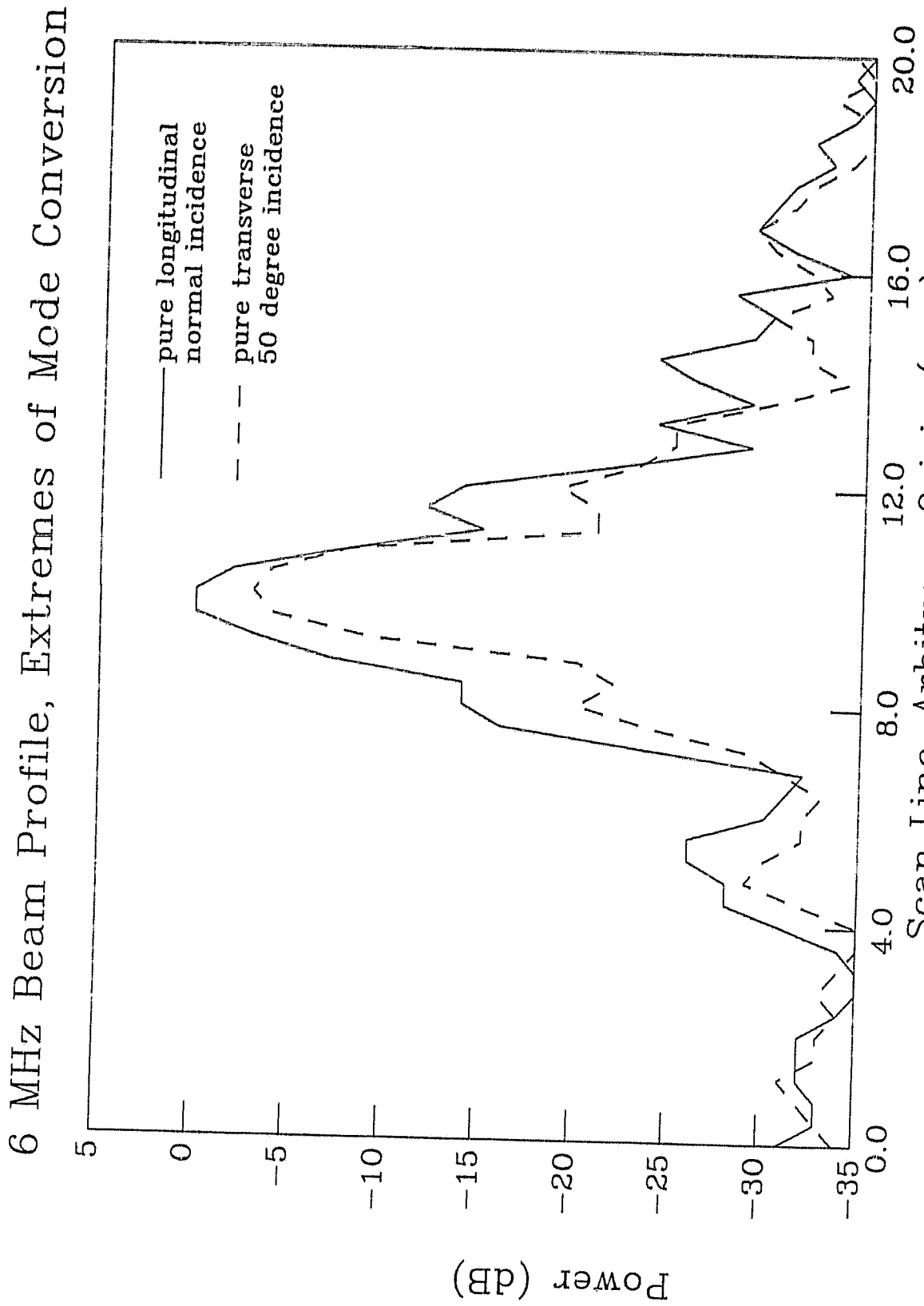

Figure 5 – Comparison of beam profile of "pure" longitudinal mode (0° incidence) versus "pure" transverse mode (50° incidence) in Lucite.

with the sidelobes on the shear wave located in the same relative position as in the water-only case. The difference in magnitude of these modes may be related to the energy converted into surface wave modes, as well as differences in the attenuation of each mode.

The exchange of energy between the transmitted longitudinal and transverse modes as the incident angle is varied is depicted in Figures 6, 7, and 8. The angles of incidence are 20, 30, and 40 degrees, respectively. The horizontal scale on each figure is self consistent, so that the actual separation of the beams can be measured. We note that near the critical angle(Figure 7) and even just beyond the critical angle(Figure 8), there is appreciable energy arriving at the appropriate time for longitudinal waves. This "smearing" of the longitudinal peak, as well as the existence of energy in longitudinal waves beyond the critical angle support the view of a finite ultrasonic beam as a superposition of an angular distribution of plane waves. Thus for any angle of incidence there are some plane waves, albeit small in magnitude, which do not exceed the critical angle. When the majority of the plane waves were near the critical angle, where small variations in incident angle result in dramatic variation in transmitted angle, these waves experience refraction, which results in an angular distribution of energy.

Conversely, this angular distribution interpretation suggests that there is always some amount of energy incident at or beyond any of the critical angles of the material. The next section of the report discusses the implications of one such angle, the Rayleigh critical angle.

IV. Bounded Beam Surface Effects

The scattering of a bounded acoustic wave from a smooth liquid-solid interface has been studied in the past few years by several investigators. One most interesting effect described is a relative maximum in scattering at the Rayleigh angle. This result was reported by de Billy, Adler, and Quentin[6] for water-stainless steel and water-copper interfaces. These same investigators later observed a relative maximum

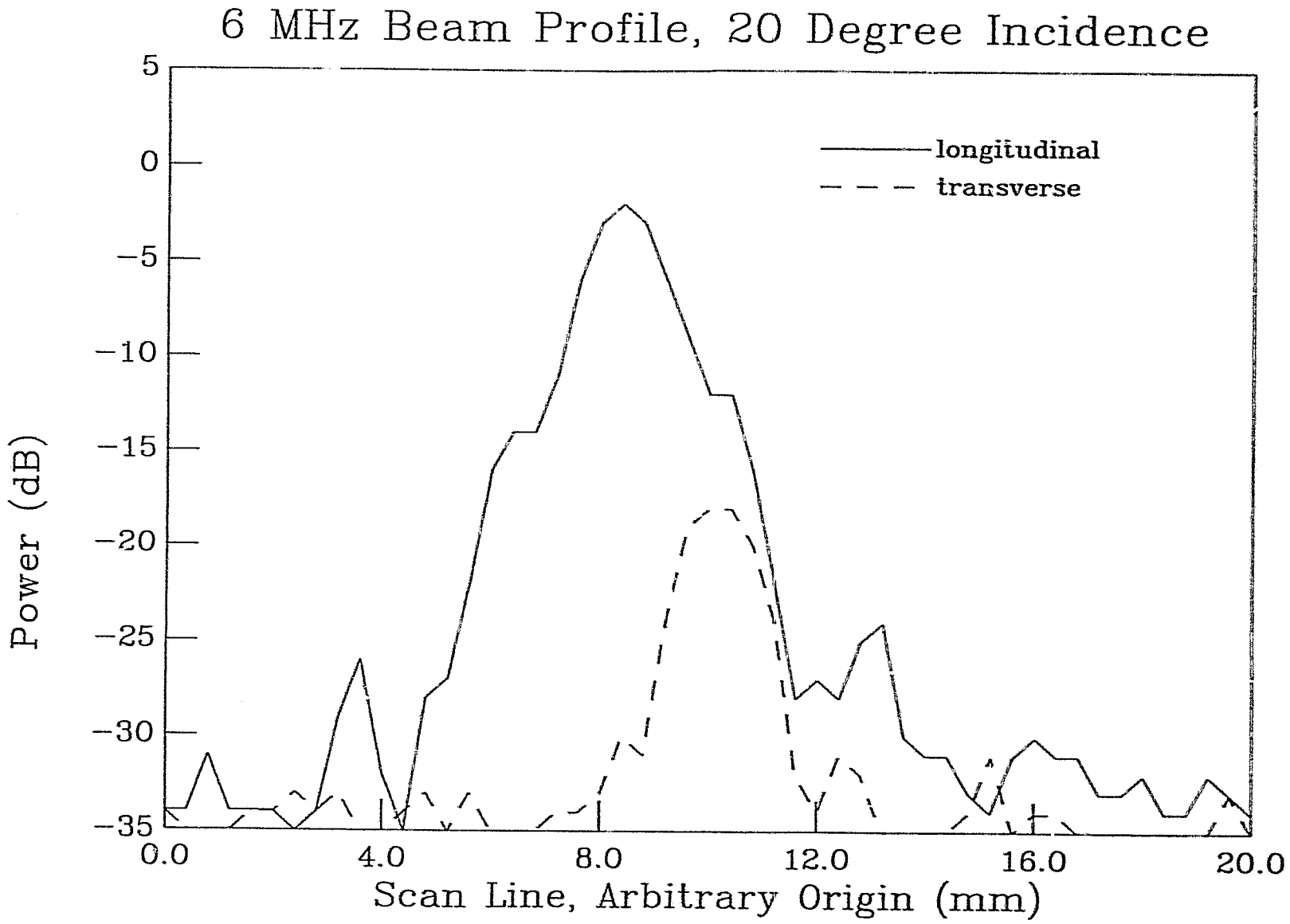

Figure 6 – Comparison of mode converted beam profiles, demonstrating the distribution of power and horizontal displacement at 20° degree incidence

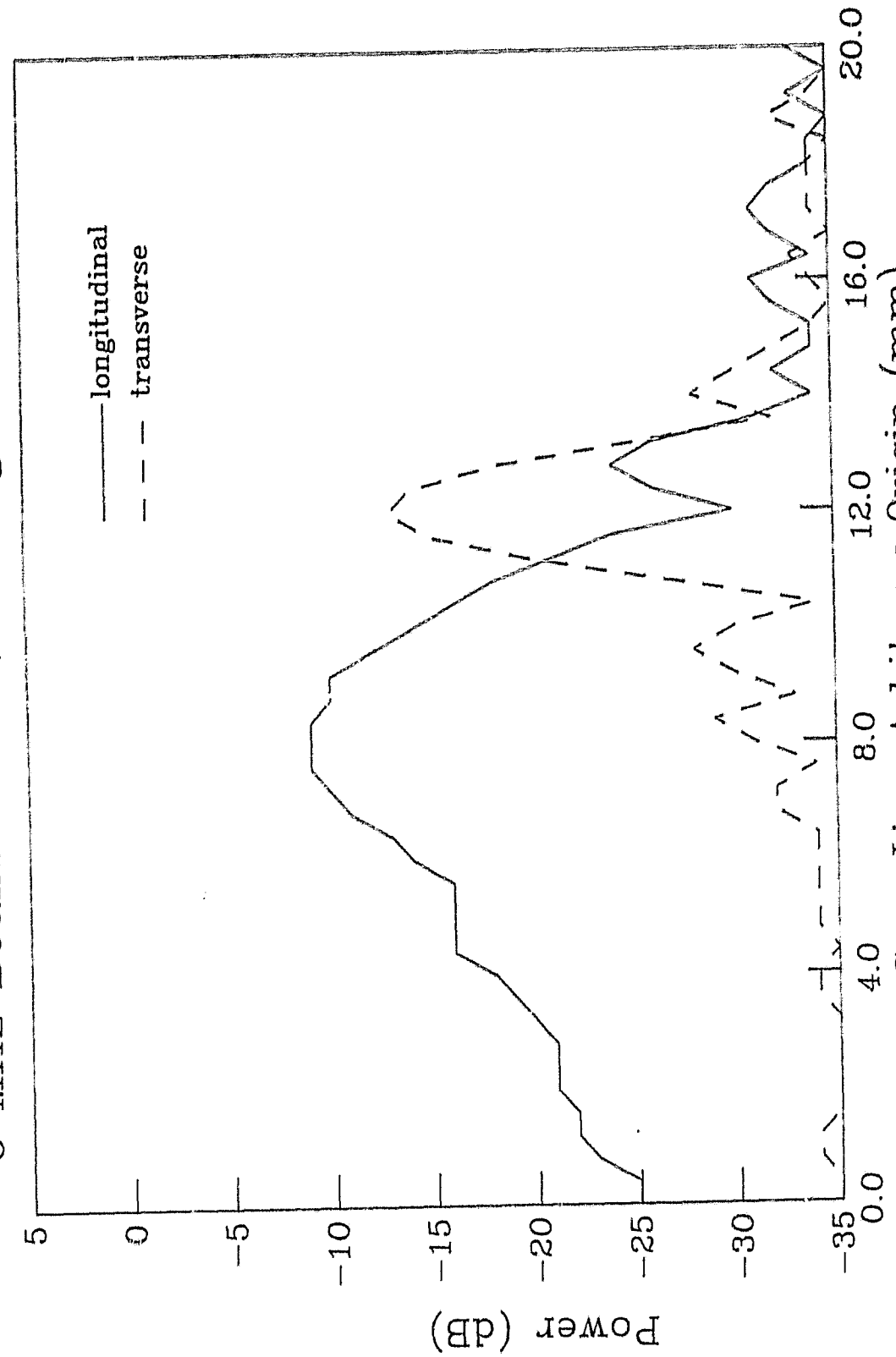

Figure 7 – Mode converted beam profiles at nominal incidence of 30°, approaching the longitudinal critical angle

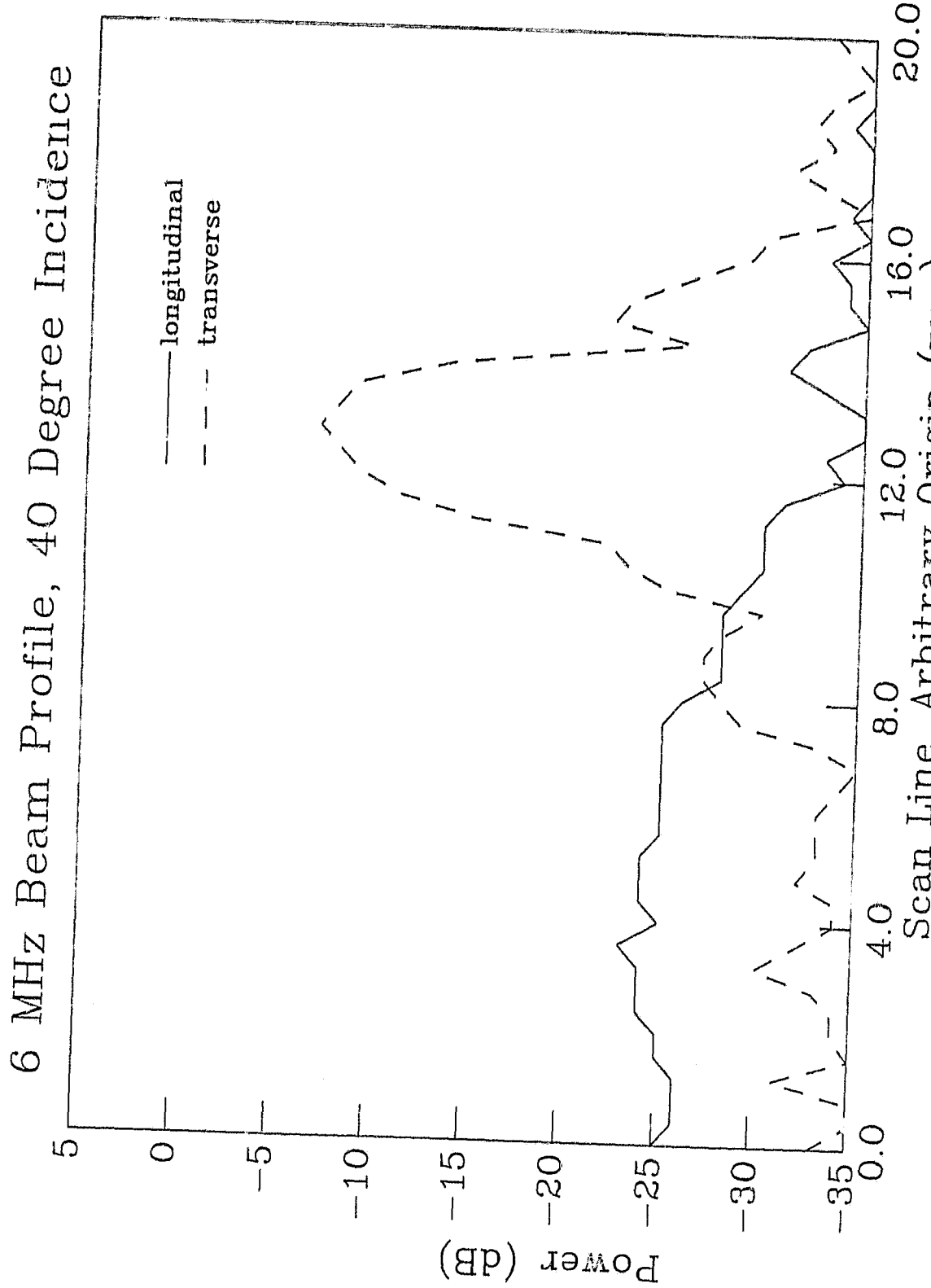

Figure 8 – Mode converted beam profiles at nominal incidence of 40°, well past the longitudinal critical angle

at both the forward and backward scattering Rayleigh angles, for any incident angle.[7] Several theoretical methods have been investigated to attempt to explain the experimental reports. Although elegant formal presentations have been developed[8,9,10] these are not as computationally straightforward as a numerical algorithm developed by Ngoc and Mayer.[4] All of the proposed theories appear to agree in the prediction that the relative maximum in backscatter at the Rayleigh angle must be related to the bounded aspect of the acoustic beam as well as to the resonant Rayleigh surface propagation mode.

The possible implications of this effect for our studies of fatigue and impact damage in composite laminates prompted us to undertake a short study of the effect. A planar stainless steel plate was insonified by a 5 MHz center frequency transducer using a broad band width pulse, as opposed to the single frequency studies reported in the literature. The incident angle was swept through 60 degrees, in one degree increments, under computer control, with the entire backscattered signal gated into a computer controlled spectrum analyzer. Several frequency components were recorded onto disc at each one degree increment. Results were calibrated with respect to the normally incident reflection. Figures 9 and 10 show the 5 MHz component of direct backscatter between 10 and 60 degrees. The vertical scale of Figure 9 is linear, that of Figure 10 is logarithmic. We note the distinct peak centered at approximately 32 degrees. The predicted Rayleigh angle for stainless steel, based on a velocity of 2891 m/sec, is approximately 31 degrees. The magnitude of the relative peak is approximately 27 dB below that of normal incidence. This magnitude, as well as the angular spread of the peak, is thought to be related to the size of the transducer and the spatial width of the ultrasonic beam. Ngoc and Mayer predict that a larger diameter transducer and tighter focusing result in narrowing the width of the peak, with transducer width paralleling variations in the relative magnitude, and tightness of focusing inversely related to the relative magnitude.

These considerations provide an approach to measuring the Rayleigh angle and hence the Rayleigh velocity. Of more direct interest to our

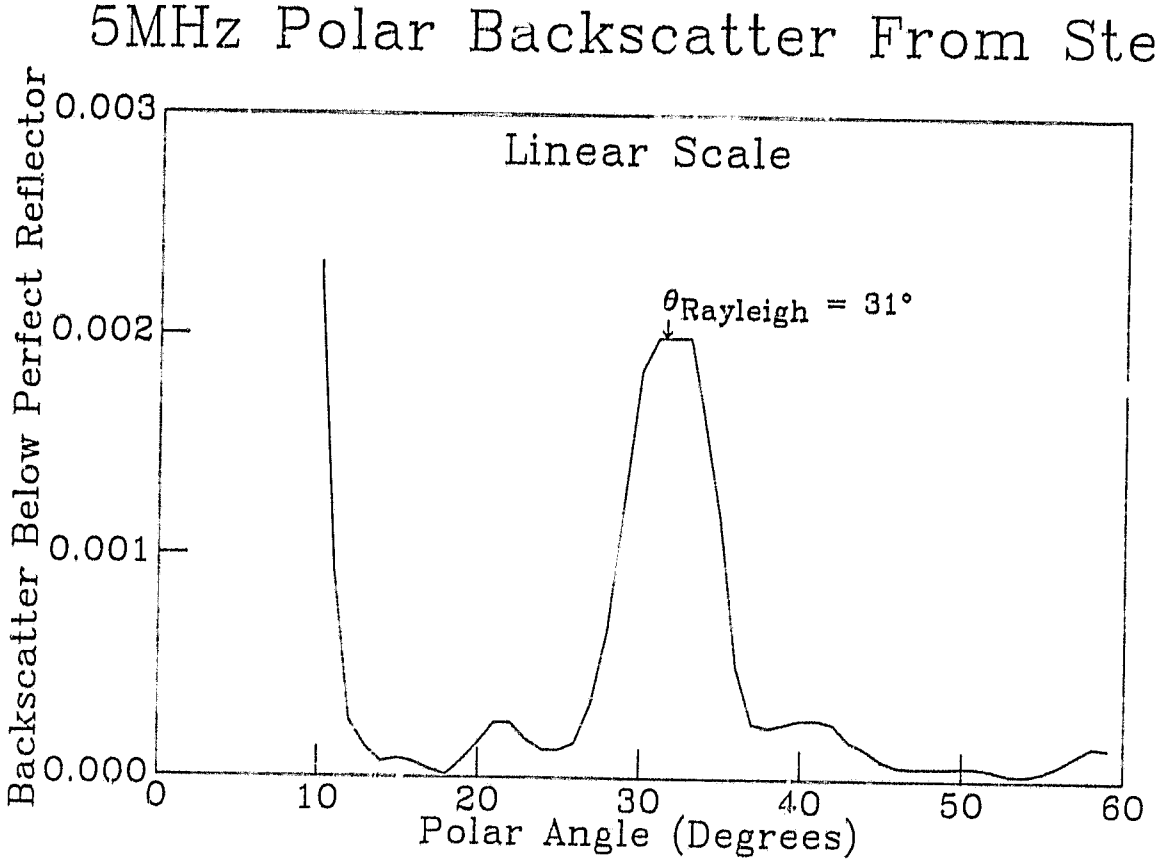

Figure 9 – Backscatter from stainless steel as a function of θ

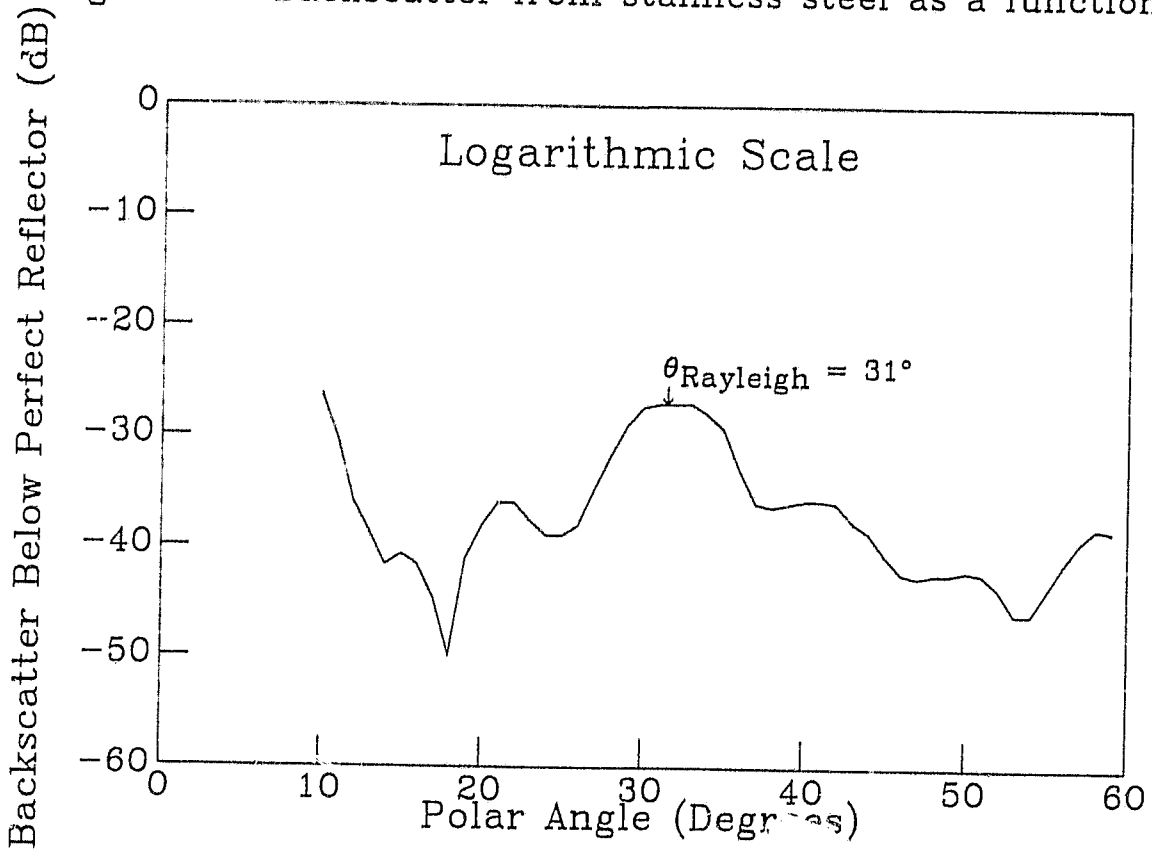

Figure 10 – Backscatter from stainless steel expressed in dB

efforts, however, is the relationship of these considerations to the polar backscatter measurements that we previously reported. Polar backscatter in graphite epoxy composites subjected to impact and fatigue damage was between 25 and 35 dB below that of a perfect (perpendicularly oriented) reflector. Clearly, if the insonifying angle was close to the Rayleigh critical angle, the bounded beam effect described above would have the potential to mask scattering from internal structures.

Further investigation of this effect may clarify the origin of difficulties in using polar backscatter on glass/epoxy specimens described in the previous report. For example, the Rayleigh velocity in fused silica glass, as determined from the Rayleigh wave velocity equation,[11] is 3400 m/sec, which leads to a Rayleigh critical angle, in water, of approximately 26 degrees. Therefore, if a glass-epoxy laminate was sufficiently glass-like ultrasonically, especially in terms of shear wave velocity, then the backscatter at the Rayleigh angle could corrupt measurements taken at a polar angle near the critical Rayleigh angle.

We are planning to conduct additional investigations of the effect of broadband vs narrow band insonification, as well as of the effects of velocity dispersion.

V. Anisotropic Mode Conversion

Considerations developed in the previous section suggest that the Rayleigh critical angle (and possibly the longitudinal critical angle as well) should be avoided when using polar backscatter techniques. In isotropic media these angles can be calculated or measured straightforwardly. In contrast, in anisotropic materials such as composite laminates the values of these critical angles are markedly dependent upon the polar and azimuthal angles of the insonifying transducer, as defined in Figure 1.

The division of power between the modes is very important for the interpretation of quantitative nondestructive evaluation, especially in the calculation of quantitative backscatter coefficients, where the spatial energy distribution of the beam must be folded into the

calculation.[12] The calculations in this section will be based on experimental velocity values in unidirectional graphite-epoxy composites as reported by Williams.[3] The Rayleigh angle backscattering maxima discussed in the previous section will be ignored, since the Rayleigh angle is estimated to be greater than 50 degrees, which is well beyond the range of polar angles we will consider here.

Williams and Nayeb-Hashemi measured the velocities of ultrasound in orthogonal directions in unidirectional graphite epoxy. As one would anticipate the velocities were fastest for propagation parallel to the fibers and slowest for propagation perpendicular. For example, the longitudinal velocity parallel to the fibers was 8400 m/sec and the perpendicular longitudinal velocity was 2800 m/sec. In general, the transverse velocities depend on the polarization as well as the propagation direction, varying between 1270 m/sec for the slowest perpendicular orientation (both propagation and displacement perpendicular to fibers) to 2000 m/sec for the parallel orientation (propagation parallel to fibers, displacement perpendicular to the fibers).

A detailed study of the exact functional dependence of the velocities on θ and ϕ in such an inhomogeneous, anisotropic medium is not consistent with the goals of the current research. However, some insight may be gained into the distribution of power in mode conversion by making a few simple approximations. First we assume that the velocities vary smoothly as θ and ϕ vary, perhaps sinusoidally. Secondly, we assume that the plane wave approximation holds so that the coefficients developed in section three can be used by replacing the constant velocities with the appropriate function of θ and ϕ.

The velocities calculated under the first assumption are depicted in Figures 11 and 12. Figure 11 contains families of curves representing the transverse velocity at fixed polar angles plotted as functions of azimuthal angle. The curves are shown for polar angles of 5, 10, 15, 20, 25, and 30 degrees. Although the azimuthal variation is significant, the variation with polar angle is less dramatic, since the range of polar angles is well away from the critical angle for shear waves.

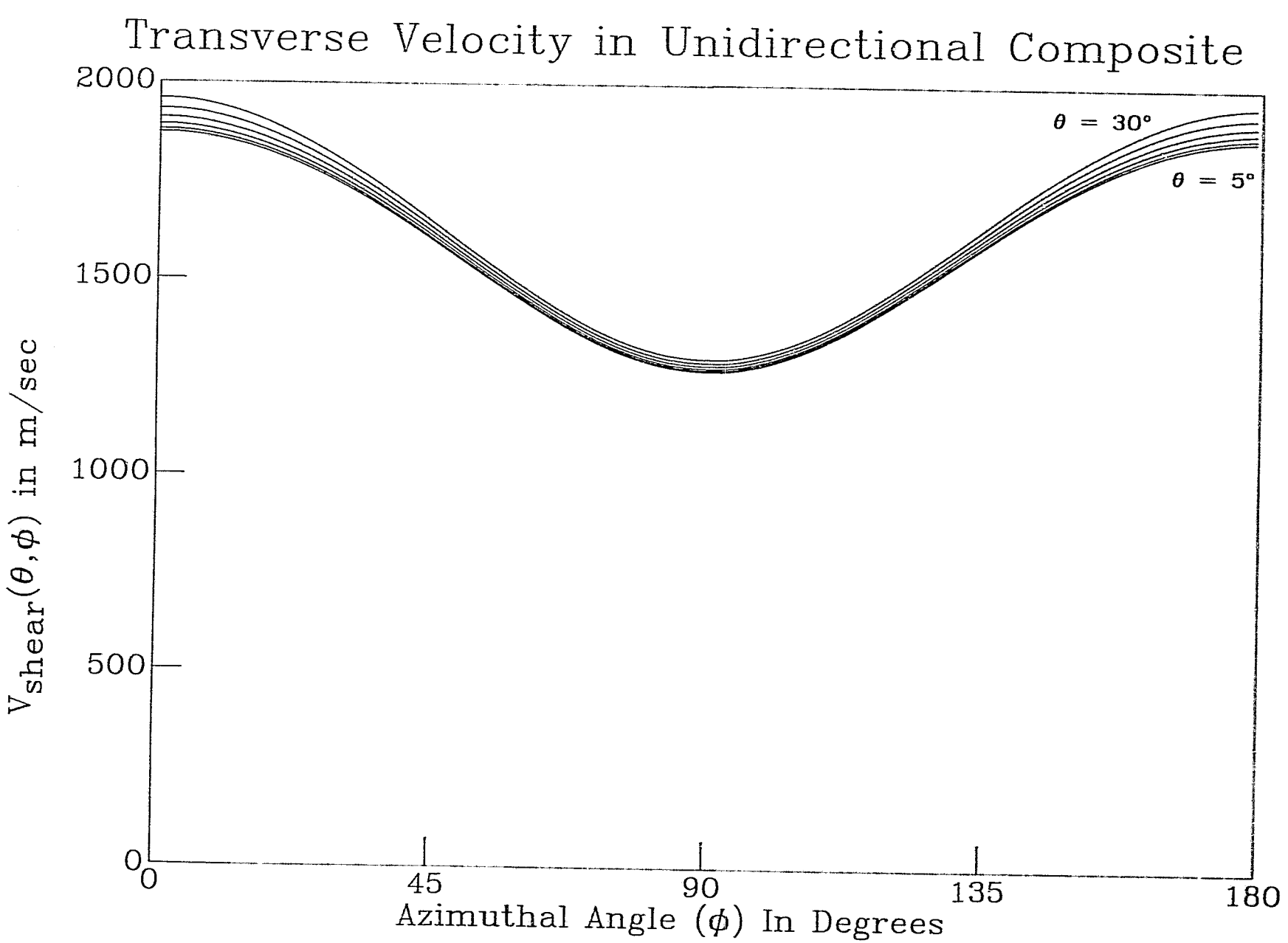

Figure 11 – Estimate of the anisotropic transverse wave velocity in a 0° graphite/epoxy composite, for constant θ ranging from 5° to 30° by 5°

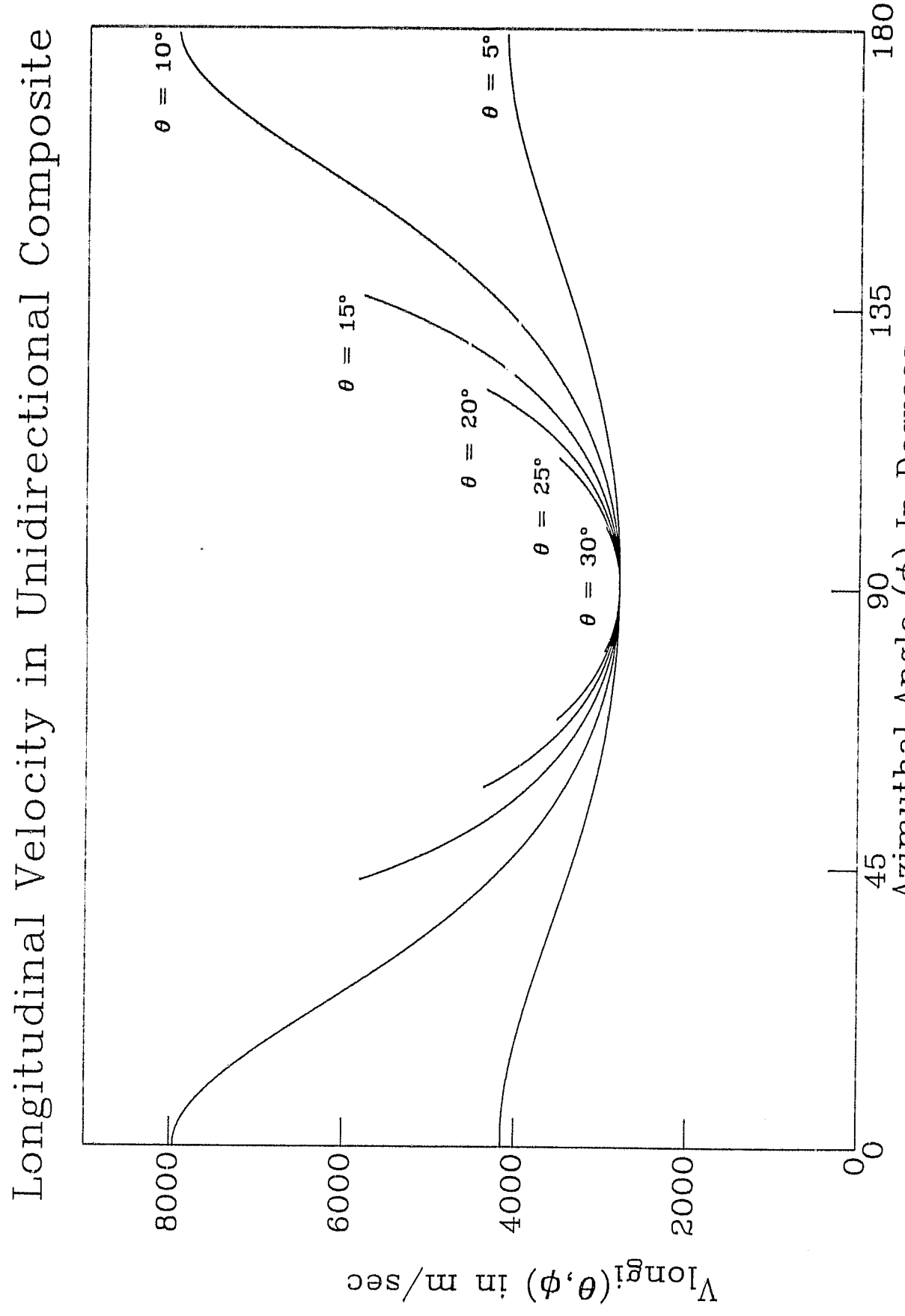

Figure 12 – Estimate of the anisotropic longitudinal wave velocity in a 0° graphite/epoxy composite, for constant θ ranging from 5° to 30° by 5°

Figure 12 depicts similar families of curves corresponding to the longitudinal velocity for polar angles of 5 degrees through 30 degrees as in Figure 11. As the polar angle increases, the range of azimuthal angle over which the longitudinal wave exists decreases resulting in the progressively narrower constant θ curves in Figures 12 through 16. This result is illustrated in Figure 13 in which the longitudinal critical angle is plotted as a function of ϕ. Clearly this variation in $\theta_{critical}$ will have a significant impact on the proper design of polar backscatter measurements.

We now apply the second assumption and utilize these velocities in the power coefficients from Section III. For simplicity we ignore the longitudinal mode for $\theta > \theta_{critical}$, under the reasonable approximation that most of the power will be in a transmitted transverse mode for those angles. Figures 14, 15, and 16 display families of curves for polar angles of 5 degrees through 30 degrees in 5 degree increments used in Figures 11 and 12. Each curve represents the fractional power in that mode, for the specified polar angle , as a function of azimuthal angle. Figure 14 depicts the power in the reflected longitudinal mode, which exhibits considerable variation with ϕ, especially near the critical longitudinal angle for that ϕ. Figure 15 plots the power in the transmitted longitudinal mode. Figure 16 displays the power in the transmitted transverse mode. Both transmitted modes show substantial variation near the critical angle.

The results of these elementary calculations have several implications. First the amount of power reflected from the surface depends significantly on the polar and azimuthal angles especially near the local critical angle. This signal can contribute significantly to the total polar backscatter. This combined with the implications of the Rayleigh angle effect described in section IV suggests that the polar backscatter technique in composites is not totally free of surface effects. We note, however, that with care, these effects can be minimized. Further consideration of improvements to the polar backscatter technique in order to reduce surface effects is under way. A second implication is the dramatic variation in the longitudinal critical

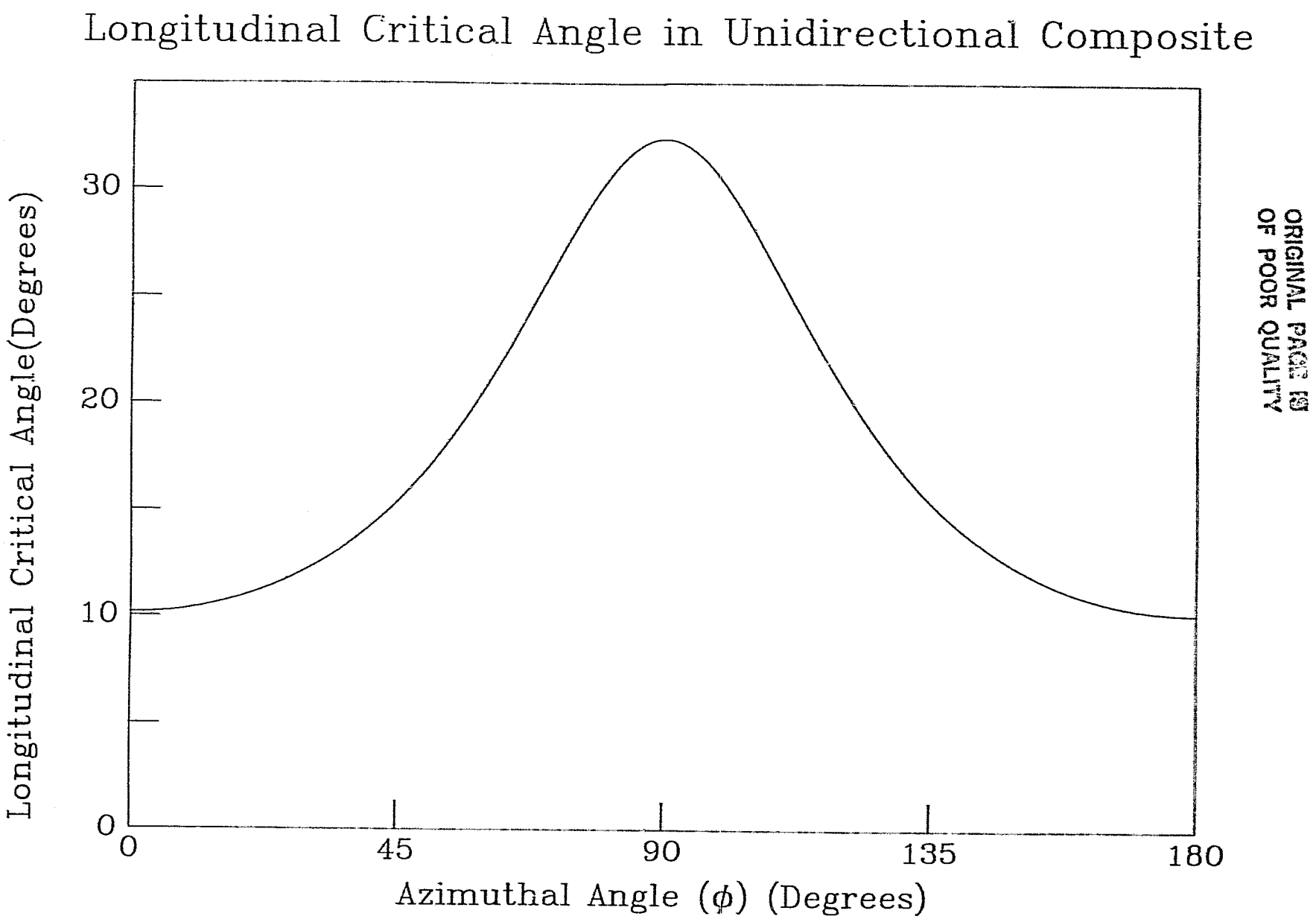

Figure 13 – Critical angle for longitudinal plane waves in a unidirectional graphite–epoxy composite as a function of ϕ

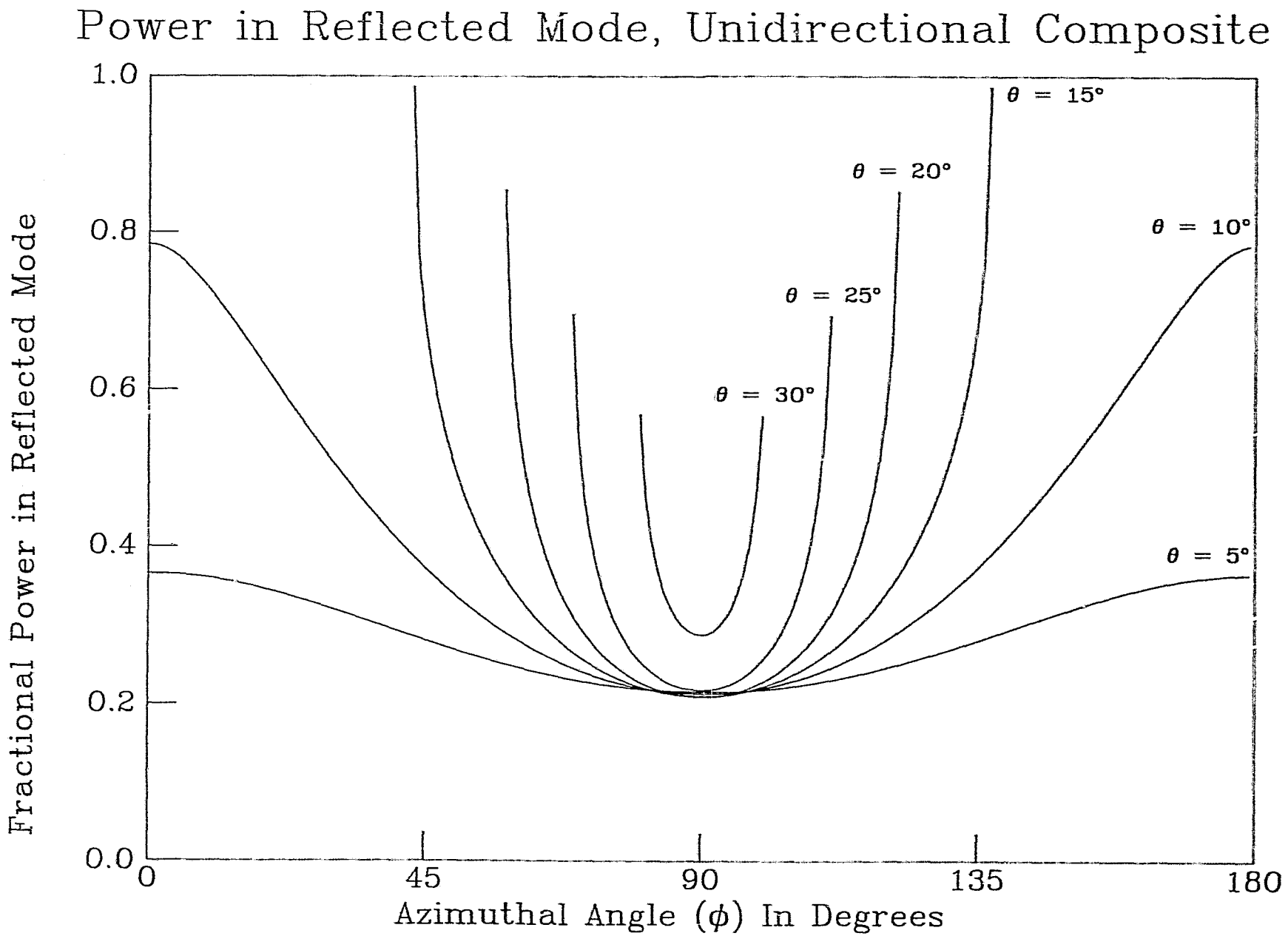

Figure 14 — Power reflected from unidirectional graphite/epoxy as a function of ϕ and θ, displayed for constant θ ranging from 5° to 30° in 5° increments

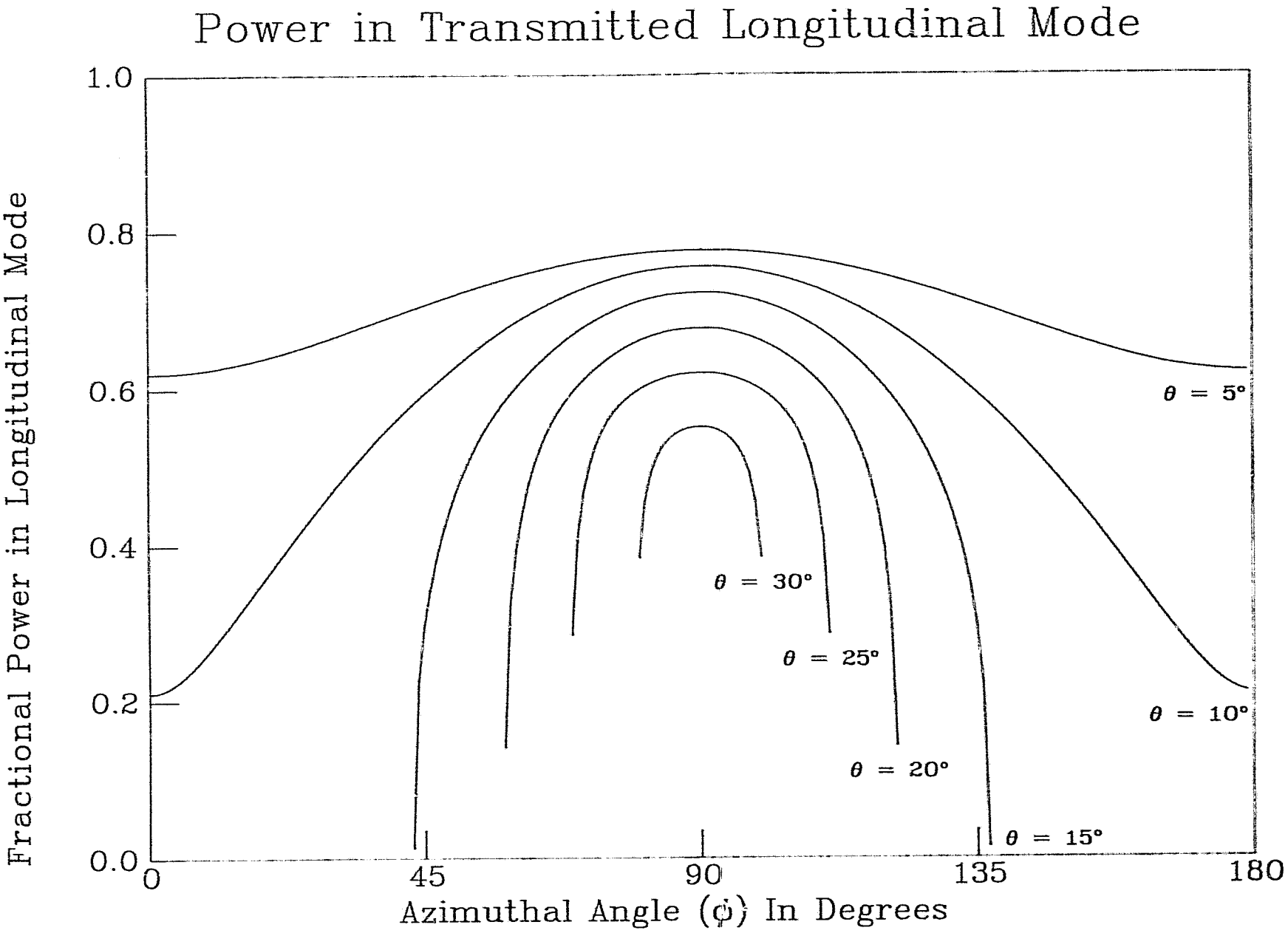

Figure 15 – Power in transmitted longitudinal mode in graphite/epoxy as a function of ϕ and θ, displayed for constant θ ranging from 5° to 30° in 5° increments

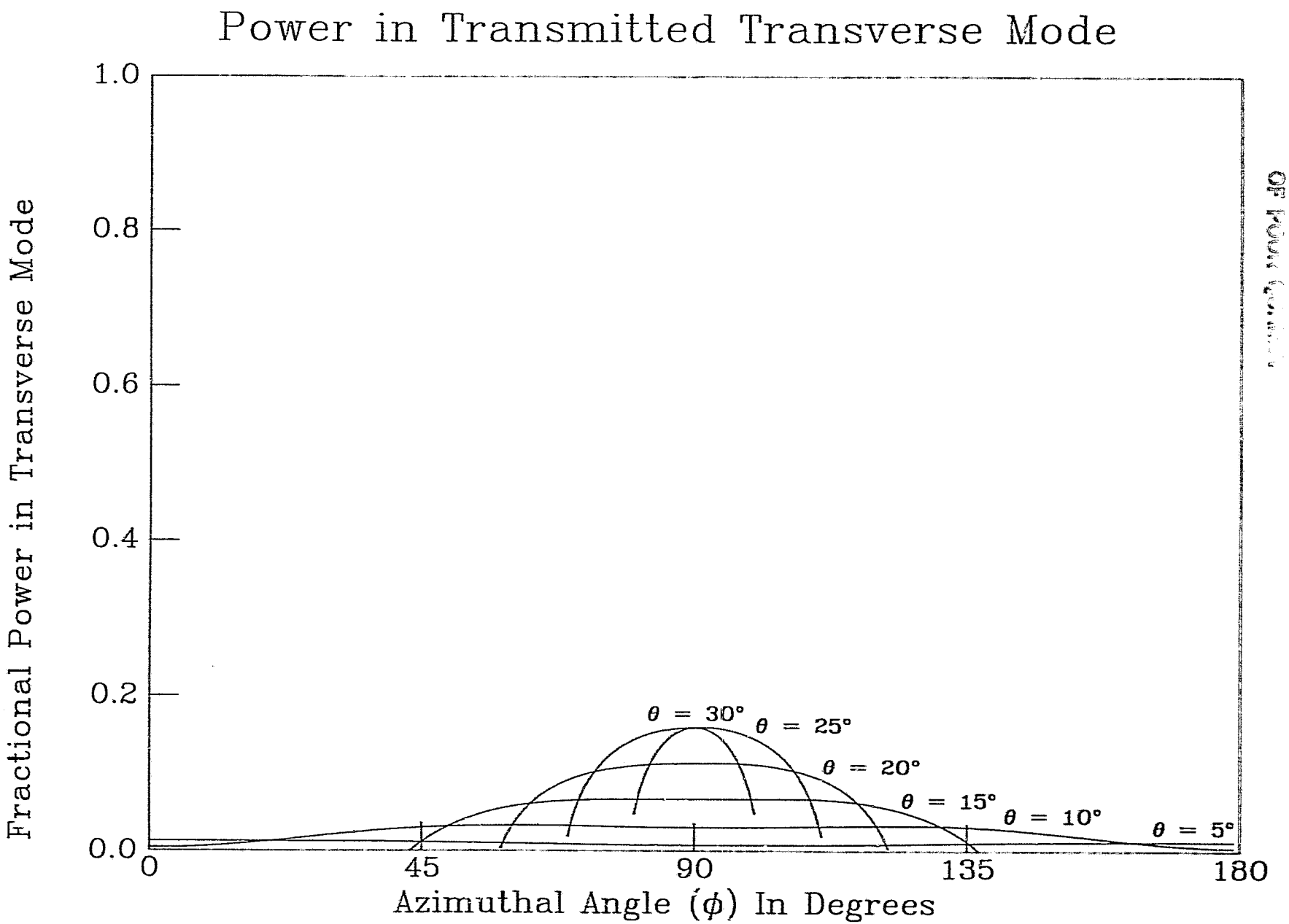

Figure 16 – Power in transmitted shear mode in graphite/epoxy as a function of ϕ and θ, displayed for constant θ ranging from 5° to 30° in 5° increments

angle. For $\theta > \theta_{critical}$, most of the power is in the transverse mode, with some power in surface waves and more in the longitudinal mode. The two regimes defined by $\theta < \theta_c$ and $\theta > \theta_c$ can be achieved at the same polar angle merely by rotating the azimuthal angle. Thus the calculation of the backscatter coefficients from the measured backscatter transfer function requires special attention under these conditions. In addition, the scattering properties exhibited by zones of damage differ depending upon the interrogating sonic mode. We plan further investigations of the effects of mode conversion in anisotropic media and the scattering properties of the different modes.

VI. Programmable Gate Circuit

Work in this and other laboratories has demonstrated the potential value of quantitative measurements of the slope of the attenuation for the nondestructive evaluation of composite materials. The transmission techniques used to date may not be feasible in many circumstances, leading to a demand for techniques of estimating the attenuation from reflected ultrasound. A number of such techniques have been proposed.[13,14,15,16]

One such technique involves measuring the shift of the centroid of the frequency spectrum of the insonifying beam as a function of depth in the attenuating medium. This approach requires a knowledge of the frequency spectrum from a number of depths, obtained either by digitization of the time domain signal and subsequent processing, or by gating appropriate segments of the signal into an analog spectrum analyzer, from which the desired spectra can be recorded directly.

Figure 17 is a sketch of a typical measurement. The symbol W represents the width or duration of the gated segment and D is the overall time delay to the beginning of the gate. The width of the gate is selected and the delay moved through the sample so that the spectrum from each depth can be recorded. We intend to use this system to estimate the slope of the attenuation in a very thick and highly attenuating sample of graphite/epoxy composite cut from a tag-end of the filament wound casing being tested for the Shuttle solid rocket motor.

Use of Programmable Gate

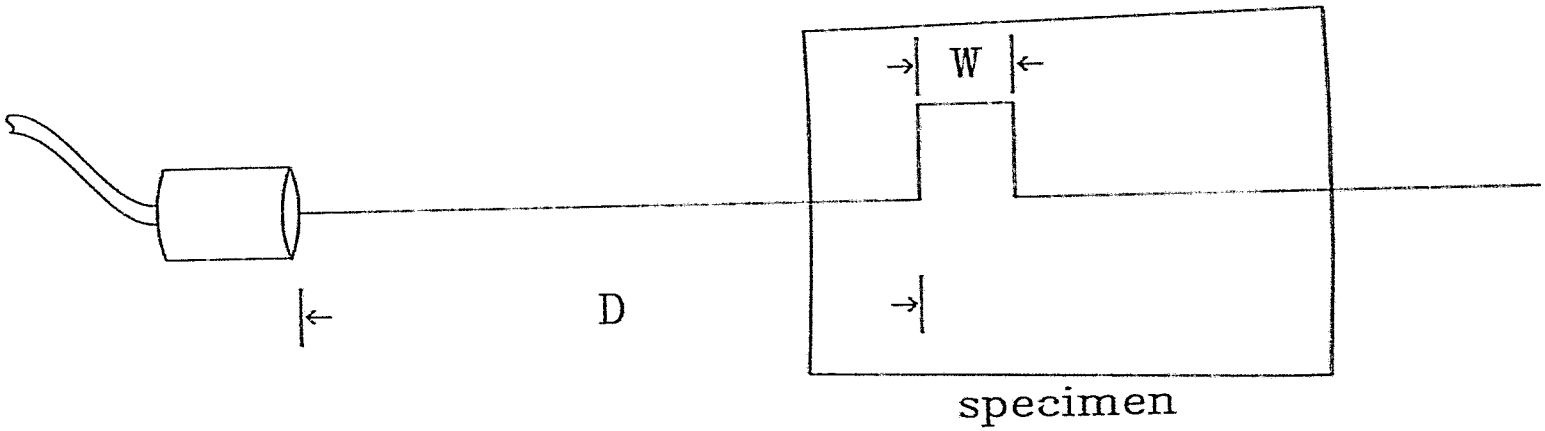

Figure 17 – Schematic representation of backscatter measurement utilizing a programmable gate.

The circuit to achieve this programmable gate is depicted by the block diagram of Figure 18. The circuit was constructed on a Hewlett-Packard Multiprogrammer Breadboard Output Card(model 69380A). This breadboard card stores 12 bits of data from the computer using built-in data latches. The circuit can be visualized as three stages built around a timing source. The timing source for this application is a 20.000 MHz K1114AM crystal oscillator. The three stages consist of a time delay counter, a gate width(or duration) counter, and an analog gate output.

The timing of the delay counter is derived from the 20 MHz clock by using a 74LS169 synchronous 4-Bit up/down counter as a divider, with the rate determined by a 4-bit DIP switch mounted on the board. The available delay clock rates are then between 1.3 MHz and 10 MHz. For most applications in this laboratory, 10 MHz is the preferred rate. This clock rate drives a 12 bit delay counter composed of three 74LS169 chips set up in cascading 4-bit stages. The counter is enabled and commences counting down by an external trigger, which triggers a 74123 one-shot into the J-port of a 74H73 high speed J-K flip flop. When the delay counter finishes, the carry out pulse triggers two 74123 one-shots, one of which reloads the delay data from the latches, while the other toggles the K input of the delay counter flip-flop, terminating counting. This termination pulse is also directed to the J input of a second flip-flop, which initiates the gate width counter and serves as the source of a TTL gate of the appropriate delay and duration.

The gate duration is determined by 8 bits run at 20MHz. The 8-bit information can be entered by hand via DIP switches on the board, or programmed via a digital output card. The gate width counter consists of two 74LS169 chips in cascade, much as the delay counter was constructed. The carry output, upon completion of the countdown, triggers a one-shot which reloads the width data and toggles the K input of the flip-flop, disabling the counter and terminating the TTL gate.

The TTL gate requires some analog shaping and buffering. The Q output of the J-K flip-flop is run through a LM318 Op-Amp set up as an

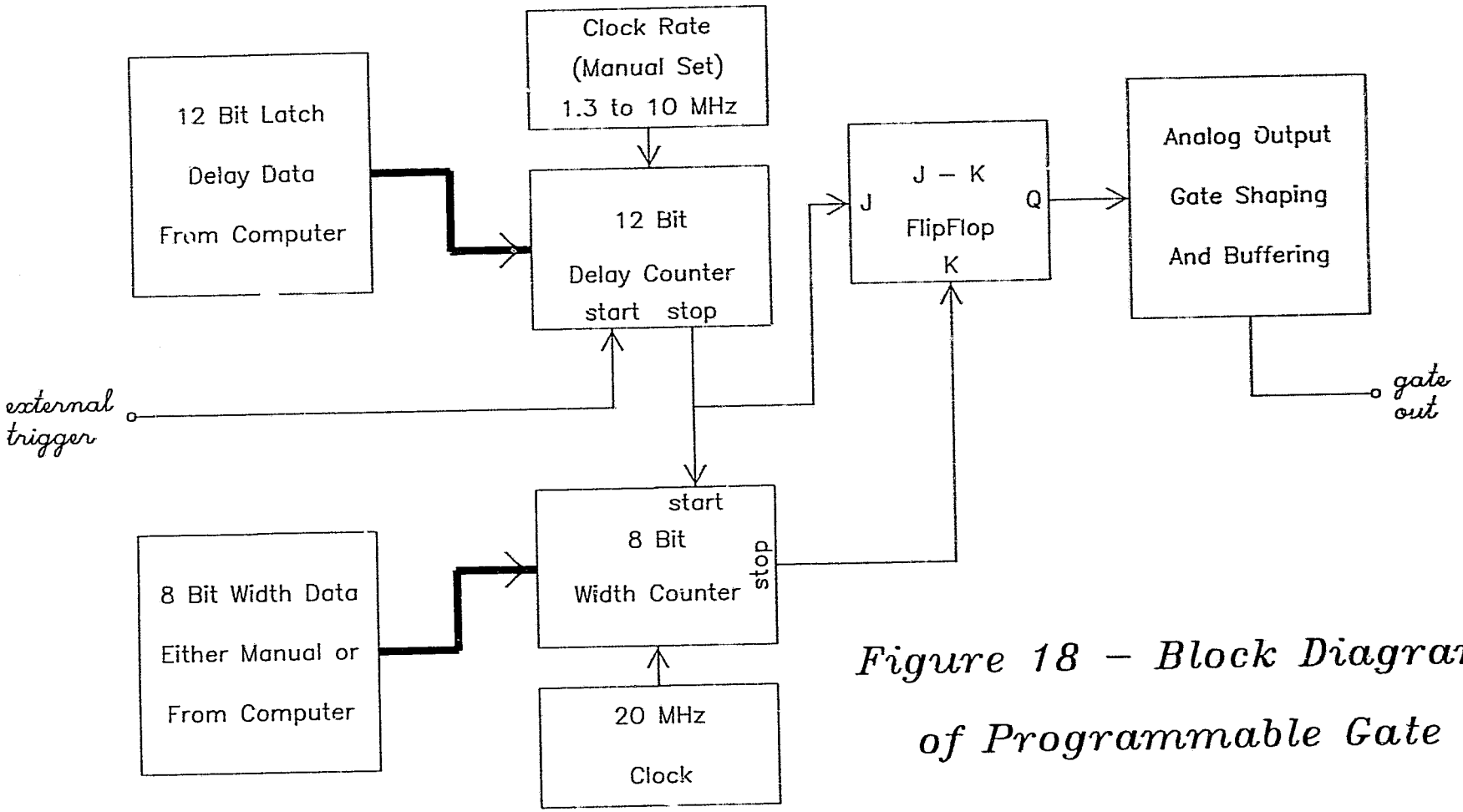

Figure 18 – Block Diagram of Programmable Gate

inverting discriminator, driving anything below 1.5 volts("on") to 15 volts and anything above 1.5volts ("off") to -15 volts thus eliminating "ringing" on the TTL signal. The resulting signal is clipped to approximately 5 volts using a Zener diode and the resulting gate is buffered through a 2N2222 transistor to supply the necessary drive levels.

The circuit so described provides a nicely shaped gate between 0.6 and 12.4 microseconds in duration, with a maximum delay (at 10 MHz) of 409 microseconds. The software required to drive the gate is very simple and allows quick and accurate placement of the gate under control of our LSI 11/23 or HP9825 computers.

VII. Conclusions

The main thrust of this report has been the discussion of some surface effects which may influence polar backscatter measurements, and the implications of mode conversion in calculating a quantitative backscatter coefficient. Further study of the details of mode conversion in inhomogeneous anisotropic media is needed to enhance our continuing study of the backscatter coefficient in composite-laminates. The boundedness of the insonifying beam may prove troublesome for polar backscatter in some media, especially near the Rayleigh angle. With some knowledge of the material under investigation, the troublesome effects of the bounded beam can be minimized by selecting polar angles away from the critical Rayleigh angle.

References

1. J. Krautkramer and H. Krautkramer, Ultrasonic Testing of Materials, Springer Verlag, New York, 1969.

2. T.D.K. Ngoc and W.G. Mayer, "A General Description Of Ultrasonic Nonspecular Reflection and Transmission Effects For Layered Media," IEEE Trans. Sonics and Ultrasonics, vol. SU-27, pp. 229-235, 1980.

3. J.H. Williams, Jr. and H. Nayeb-Hashemi, "Ultrasonic Attenuation and Velocity in AS/3501-6 Graphite/Epoxy Fiber Composite," NASA

Contractor Report 3180, 1979.

4. T.D.K. Ngoc and W.G. Mayer, "Theoretical Prediction of a Backscattering Maximum at Rayleigh Angle Incidence for a Smooth Liquid-Solid Interface," J. Acoust. Soc. Am., vol. 75, pp. 186-188, 1984.

5. R.C. Weast ed., CRC Handbook of Chemistry and Physics, 51st edition, The Chemical Rubber Co., Cleveland, 1970.

6. M. de Billy, L. Adler, and G. Quentin, "Parameters Affecting Backscattered Ultrasonic Leaky-Rayleigh Waves from Liquid-Solid Interfaces," J. Acoust. Soc. Am., vol. 72, pp. 1018-1020, 1982.

7. L.Adler, M. de Billy, and G.J. Quentin, "Excitation of Ultrasonic Rayleigh Leaky Waves at Liquid-Solid Interface for General Angle Incidence," J. Appl. Phys., vol. 53, pp. 8756-8758, 1982.

8. H.L. Bertoni and T. Tamir, "Unified Theory of Rayleigh-Angle Phenomena for Acoustic Beams at Liquid-Solid Interface," Appl. Phys., vol. 2, p. 157, 1973.

9. M. de Billy and G. Quentin, "Backscattering of Acoustic Waves by Randomly Rough Surfaces of Elastic Solids Immersed in Water," J. Acoust. Soc. Am., vol. 72, p. 591, 1982.

10. A.N. Norris, "Back Reflection of Ultrasonic Waves from a Liquid-Solid Interface," J. Acoust. Soc. Am., vol. 73, p. 427, 1983.

11. B.A. Auld, Acoustic Fields and Waves in Solids, Vol II, Wiley Interscience, New York, 1973.

12. M. O'Donnell and J.G. Miller, "Quantitative Broadband Ultrasonic Backscatter: An Approach to Non-Destructive Evaluation in Acoustically Inhomogeneous Materials," J. Appl. Phys., vol. 52, pp. 1056-1065, 1981.

13. R.B. Kuc, "Statistical Estimation of the Acoustical Attenuation Slope for Liver Tissue," Ph.D. Thesis, Columbia University, 1977.

14. R.B. Kuc and M. Schwartz, "Estimating the Acoustic Attenuation Slope for Liver from Reflected Ultrasound Signals," IEEE Trans. Sonics Ultrasonics, vol. SU-26, pp. 353-362, 1979.

15. M. Fink, "Theoretical Study of Pulsed Echographic Focusing Procedures," Acoustical Imaging, vol. 10, pp. 437-453, Plenum, 1980.

16. M. Fink and F. Hottier, "Short Time Fourier Analysis and Diffraction Effect in Biological Tissue Characterization," Acoustical Imaging, vol. 12, pp. 493-503, Plenum, 1982.